



Contents lists available at ScienceDirect

Nuclear Engineering and Design

journal homepage: www.elsevier.com/locate/nucengdes



Thermal hydraulic design of a hydride-fueled inverted PWR core

J.A. Malen^{a,*}, N.E. Todreas^b, P. Hejzlar^b, P. Ferroni^b, A. Bergles^c

^a University of California, Berkeley, Department of Mechanical Engineering, Berkeley, CA 94720, United States

^b Massachusetts Institute of Technology, Department of Nuclear Engineering, Cambridge, MA 02139, United States

^c Massachusetts Institute of Technology, Department of Mechanical Engineering, Cambridge, MA 02139, United States

ARTICLE INFO

Article history:

Received 2 August 2007

Received in revised form 10 June 2008

Accepted 21 February 2009

Available online xxx

ABSTRACT

An inverted PWR core design utilizing U(45%, w/o)ZrH_{1.6} fuel (here referred to as U–ZrH_{1.6}) is proposed and its thermal hydraulic performance is compared to that of a standard rod bundle core design also fueled with U–ZrH_{1.6}. The inverted design features circular cooling channels surrounded by prisms of fuel. Hence the relative position of coolant and fuel is inverted with respect to the standard rod bundle design. Inverted core designs with and without twisted tape inserts, used to enhance critical heat flux, were analyzed. It was found that higher power and longer cycle length can be concurrently achieved by the inverted core with twisted tape relative to the optimal standard core, provided that higher core pressure drop can be accommodated. The optimal power of the inverted design with twisted tape is 6869 MW_t, which is 135% of the optimally powered standard design (5080 MW_t—determined herein). Uncertainties in this design regarding fuel and clad dimensions needed to accommodate mechanical loads and fuel swelling are presented. If mechanical and neutronic feasibility of these designs can be confirmed, these thermal assessments imply significant economic advantages for inverted core designs.

© 2009 Elsevier B.V. All rights reserved.

1. Introduction

Previous studies assessed the potential to reduce the cost of electricity by implementing U–ZrH_{1.6} in PWRs, both by backfitting existing plants and by designing new cores (Malen et al., 2004; Shuffler et al., this issue-a, this issue-b). These studies, which assumed that the fuel would be arranged in rod bundles (referred to as “standard design”), concluded that significant cost savings for U–ZrH_{1.6} compared to oxide fuel could not be achieved in grid supported PWRs, primarily because the power and energy generation per core loading for both fuels with square arrays supported by grid spacers are similar.¹ Other hydride fuels would actually offer advantages compared to U–ZrH_{1.6}, including increased heavy metal density and lower hydrogen release at high temperature (Greenspan et al., this issue). In spite of this, for the present inverted fuel design investigation only U–ZrH_{1.6} was assessed, based on its use in TRIGA reactors and availability of thermophysical properties.

This paper investigates the implementation of U–ZrH_{1.6} in PWRs, no longer assuming a standard design, but an inverted design. In particular, the study: (1) estimates the performance of U–ZrH_{1.6}

inverted geometry and (2) compares such performance to that of an optimally powered standard fuel rod design also fueled with U–ZrH_{1.6}, to assess the relative economic feasibility of the inverted design.

The inverted design consists of prismatic blocks of fuel perforated with non-communicating cylindrical coolant channels, similar to the fuel concept proposed for gas cooled fast reactors (Pope et al., 2005). At subchannel level, the inverted geometry is characterized by two parameters, cooling channel diameter and pitch. For standard rod bundles the subchannel is a coolant channel surrounded by circular fuel rods; for the inverted design the subchannel is a circular coolant channel surrounded by a hexagonal fuel cell. The circular channels are arranged within the fuel in hexagonal close packed arrays to minimize the conduction length between the channel wall and the vertices of the fuel cell. Like in hydride standard designs, the gap between the fuel and clad is filled with a liquid metal (Pb–Bi–Sn eutectic) to enhance heat transfer, so that phenomena like fission gas release, hydrogen release and irradiation-induced fuel swelling, which are temperature-dependent, can be limited (Olander et al., this issue). Cross-sections of a standard subchannel and an inverted subchannel are shown in Fig. 1. An inverted fuel assembly consists of a hexagonal block of fuel encased in cladding, such that the clad covering the cooling channel interiors is connected at the top and bottom to perforated hexagonal lids. The sides of the fuel block are also clad to complete the enclosure. The inverted channels are only connected at the core inlet and outlet, where flow distribution is determined. The number

* Corresponding author.

E-mail address: jonmalen@berkeley.edu (J.A. Malen).

¹ Similar conclusions were drawn for hexagonal arrays with grid spacers. However, the use of a wire wrapped pin configuration did improve the thermal hydraulic performance in the low pitch-to-diameter ratio regions where hydride fuel has significant neutronic advantages over oxide fuel (Diller et al., this issue).

Nomenclature

A	cross-sectional area (m ²)
BU	burnup (MWD/kg _{HM})
CHF	critical heat flux (W/m ²)
D	diameter (m)
D _e	equivalent diameter (m)
D _{SC}	standard core fuel rod diameter (m)
D _I	inverted core cooling channel diameter (m)
f	Moody friction factor
FCR	fuel to coolant volume ratio
IC	inverted core
ICTT	inverted core with twisted tape
L	core height (m)
L _{180°}	axial length required for TT to complete a 180° rotation
MDNBR	minimum departure from nucleate boiling ratio
m _{HM}	mass of heavy metal in core (kg)
P	pitch (m)
P/D	pitch-to-diameter ratio
ΔP	pressure drop (MPa)
q''	heat flux (W/m ²)
R	radius (m)
Re	Reynolds number
SC	standard core
t	thickness (used for gap, clad and fuel web) (m)
T	temperature (°C)
T _{cycle}	cycle length (months)
TT	twisted tape
V	coolant velocity (m/s)
y	L _{180°} /D _I
α	A _F /A _{FG} ratio
β	A _F /A _{FGC} ratio
μ	viscosity (N s/m ²)
ρ	density (kg/m ³)

Subscripts

CI	clad inner radius or diameter
CO	clad outer radius or diameter
F	fuel
FG	fuel + gap
FGC	fuel + gap + clad
I	IC and ICTT
IC	inverted core
ICTT	inverted core with twisted tape
EA	equivalent annulus
Max	maximum fuel temperature
ref	reference PWR core
SC	standard core
CI	clad inner radius or diameter
TT	twisted tape

and height of subchannels within each assembly, and the number of assemblies in the core may vary and their optimization is not addressed here. Rather the analysis presented here is performed on a single inverted subchannel, as described in Section 3. Twisted tape inserts may be welded to the inside surface of the circular coolant channel (see Fig. 1) to enhance the CHF at the expense of added pressure drop. We have evaluated the performance of the inverted geometry with and without twisted tapes.

Control rod design, not addressed in this work, could be in the form of BWR-like control rods consisting of three blades spaced by a 120° angle and inserted in the water gaps between the hexagonal assemblies.

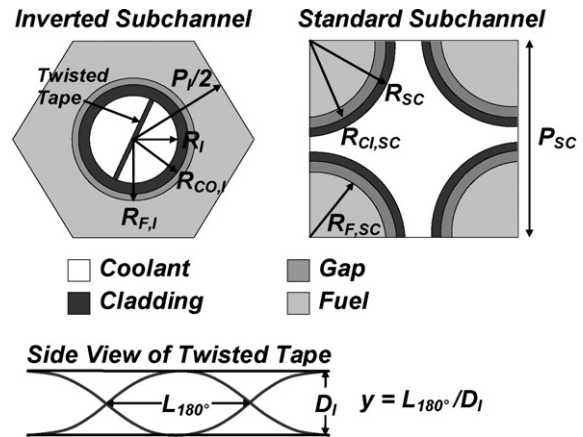


Fig. 1. Geometry of inverted and standard subchannels.

Characteristics of the inverted design that prompted our investigation include reduction of vibration concerns, ability to enhance critical heat flux (CHF) performance by means of twisted tape inserts, and potential for reduced pressure drop relative to rod bundles. Furthermore, the inverted geometry may afford high power density for geometries that also offer high burnup and heavy metal loading. These three traits are not simultaneously optimized by the standard fuel rod core designs. The possibility of Zr–U assembly blocks to be drilled before hydration is performed, together with the low fission gas release characterizing U–ZrH_{1.6} (Simmnad, 1981), make this fuel type suitable for the inverted geometry.

2. The parametric study design space

The study presented here is a parametric study of inverted and standard subchannel geometries, from which whole core properties were calculated by means of geometric relations and conservative assumptions on the core radial power distribution. Section 3 describes the analysis methodology in detail. Three designs utilizing U–ZrH_{1.6} were studied: (1) the standard core (SC), (2) the inverted core (IC), and (3) the inverted core with twisted tape inserts (ICTT).

The parametric study was performed over a range of geometries to identify the optimal combination of cooling channel pitch and diameter for each of the three designs. The geometry range was identified in terms of fuel to coolant volume ratios (FCR) and fuel areas per subchannel (A_F). These variables enable a direct comparison of the U–ZrH_{1.6} fueled standard and inverted designs. Furthermore, neutronic design is highly dependant on FCR, so it is appropriate to compare standard and inverted designs of equivalent FCR.² Geometries within the range 0.3 ≤ FCR ≤ 2.0 and 20 mm² ≤ A_F ≤ 150 mm² were evaluated for each of the three designs. These ranges correspond to P/D ratio ranges of 1.65 ≥ (P/D)_{SC} ≥ 1.04 and 4.13 ≤ (P/D)_I ≤ 1.84 for the standard and inverted geometry, respectively. Geometric relationships based on FCR and A_F are summarized in Table 1.

Fig. 2 shows how FCR varies with P/D for both standard and inverted designs. FCR and A_F of the reference core are FCR_{ref} = 0.59 and A_{F,ref} = 52.1 mm². Geometric parameters and operating conditions, listed in Table 2, are from a typical UO₂ fueled PWR.

² We have assumed that the twisted tape does not impact neutronic performance, both because of its small volume, i.e., a 0.4 mm thick tape insert will occupy only ~4% of a channel that is 12 mm in diameter, and because of the low neutron absorption material, Zircaloy, specified for its fabrication. The twisted tape is assumed to be welded to the cooling channel inner surface, and to have small thickness compared to the channel inner diameter.

Table 1
Geometric relationships between P/D , FCR, β , A_F , and D_e .

Design	Geometric relationship
All (SC, IC, ICTT)	$\alpha = \frac{A_F}{A_{FG}} = 0.950$ $\beta = \frac{A_F}{A_{FC}} = 0.736$
SC	$\left(\frac{P}{D}\right)_{SC} = \sqrt{\frac{\pi}{4} \left(\frac{\beta}{FCR} + 1\right)}$ $D_{e,SC} = \frac{2\sqrt{\beta A_{F,SC}}}{FCR\sqrt{\pi}}$
Inverted (IC, ICTT)	$\left(\frac{P}{D}\right)_I = \sqrt{\frac{\pi}{2\sqrt{3}} \left(\frac{FCR}{\beta} + 1\right)}$ $D_{e,IC} = 2\sqrt{\frac{A_{F,I}}{\pi FCR}}$ $D_{e,ICTT} = \frac{2\pi}{\pi+2} \sqrt{\frac{A_{F,I}}{\pi FCR}}$

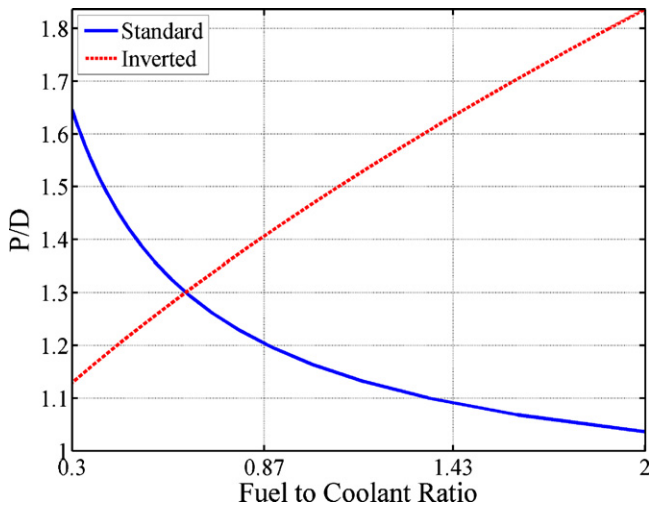


Fig. 2. Relationship of governing geometric parameters defining fuel and coolant channel arrays, for $\beta = 0.736$.

Parameters shown in italics are variables of the parametric study, while those not italicized are constant for all core designs.

3. Analysis methodology

The goal of the thermal hydraulic analysis was to determine the maximum core power attainable by all the SC, IC and ICTT geometries in the design space discussed in the previous section, subject

Table 2
Design and performance parameters of the reference oxide PWR (Seabrook UFSAR, 2002).

Parameter ^a	Value
Equivalent core radius	1.68 m
Active fuel length	3.66 m
Cladding outer diameter D_{ref}	9.5 mm
Cladding thickness	0.57 mm
Fuel-clad-gap width	0.08 mm
Square lattice pitch, P_{ref}	12.6 mm
Pitch-to-diameter ratio, P/D_{ref}	1.326
Number fuel rods per core	50,952
Core average enthalpy rise	192.1 kJ/kg
Core inlet temperature	294 °C
System pressure	15.51 MPa
Radial peaking factor ^b	1.65
Axial peaking factor	1.55
Power level	3400 MW _t
Average linear heat rate	182 W/cm

^a Parameters in italics are variables of this study. All other parameters are fixed.
^b Hottest subchannel power/average subchannel power.

to limitations on power imposed by thermal hydraulic constraints. All SC, IC and ICTT geometries were analyzed by modeling their respective hot subchannel. The thermal hydraulic code used for this analysis, i.e., VIPRE (Stewart, 1985), was interfaced with Matlab in order to: (1) quickly span the whole FCR and A_F ranges, (2) iteratively vary the channel power in order to calculate the maximum achievable power, and (3) add the corrections needed to account for the presence of design features, like the twisted tape, that cannot be implemented in a VIPRE-only model. The flow rate through the hot channel was however calculated accounting for flow distribution among all the cooling channels, so that the pressure drop imposed across the hot channel equals that across the whole core. For IC and ICTT, the VIPRE analysis was performed by modeling the inverted subchannel as an equivalent standard subchannel having the same coolant cross-section and heated perimeter as the actual inverted subchannel. However, because of the hexagonal geometry characterizing the fuel cell, the equivalent standard subchannel model was not used to calculate the temperature distribution across the hexagonal fuel cell. Rather, the equivalent annulus heat conduction approximation, described in Appendix A.3, was used for this purpose.

Geometric relations and the conservative peaking factors shown in Table 2 were then applied to the hot subchannel geometry in order to obtain whole core properties, such as total heavy metal loading and core power. In particular, the cross-sectional area available for the subchannels (needed for the calculation of the number of subchannels in the core) was taken as 90% of the total cross-section to approximate the presence of design features not explicitly modeled in this study. These primarily included the duct surrounding each fuel block, gaps needed to accommodate fuel swelling and the inter-assembly gap needed to allow assembly and control rod insertion and withdrawal.

4. Constraints of the parametric study

The maximum achievable power of a given core is defined as the highest steady state power that can be sustained without breaching a single constraint limit. The constraints considered include fuel temperature and cladding temperature during steady-state operation, minimum departure from nucleate boiling ratio (MDNBR) during an overpower event and maximum cladding temperature during a loss of coolant accident (LOCA). The coolant velocity constraint, which was applied to the SC design to limit flow induced vibrations, was not applied to IC and ICTT designs since they are assumed to inherently resist vibrations. The limits used are listed in Table 3 and a discussion of each constraint follows in this section.

Pressure drop was recorded, but not constrained, because it is not a safety concern. To predict the pressure drop for the ICTT, the friction factor was changed from a single phase straight tube friction factor to a single phase twisted tape friction factor. The twisted tape friction factor used was that recommended by Manglik and Bergles (1993):

$$f_{TT} = f_{y=\infty} \left(1 + \frac{2.752}{y^{1.29}} \right), \quad 30,000 < Re \quad (1)$$

where y is the axial length required for the tape to complete 180° twist, per unit channel internal diameter, and $f_{y=\infty}$ is the friction factor for a straight tube with a straight tape insert, herein estimated by the Colebrook correlation (Colebrook, 1939).

4.1. Steady-state fuel and cladding temperature constraints

The steady-state temperature limit chosen for U-ZrH_{1.6}, i.e., 750 °C, was fixed to limit hydrogen release, fission gas release and irradiation-induced fuel swelling. Keeping the fuel temper-

Table 3
 Summary of limits for steady state, overpower and LOCA scenarios.

Design	Steady state			Overpower transient		LOCA
	$T_{\text{fuel}} (^{\circ}\text{C})$	$T_{\text{clad}} (^{\circ}\text{C})$	V^a (m/s)	MDNBR limit	MDNBR correlation	$T_{\text{clad}} (^{\circ}\text{C})$
SC	<750	<350	<8	>1.21	W3-L	1204
IC	<750	<350	–	>1.3	Groeneveld 95 lookup	1204
ICTT	<750	<350	–	>1.3 ^b	Viskanta data ^b	1204

^a Flow induced vibrations are constrained by limiting V .
^b CHF dependence on diameter is assessed by 2 approaches.

ature below 750 °C guarantees the hydrogen partial pressure of U–ZrH_{1.6} to be below about 0.3 bar and the fission gas release fraction to be of order 10^{−3} to 10^{−4} (Simnad, 1981). A significant uncertainty accompanies hydride fuel swelling since very few experimental measurements were performed on this type of fuel. Lillie et al. (1973) indicates that, above 650 °C, U–ZrH_{1.6} shows a significant increase in irradiation-induced swelling. However, because of the limited experimental data on this subject and because of the possibility to accommodate swelling by providing sufficient dimensioning of the fuel–clad–gaps, as discussed in Section 5.2, the maximum fuel temperature was limited to 750 °C.

A steady state cladding temperature limit of 350 °C was selected for zirconium cladding to limit the oxidation layer thickness (NRC 10CFR50.46).

4.2. Vibration constraint

The coolant velocity limit of 8 m/s applied to SC derives from a detailed vibration analysis performed on SCs by Shuffler et al. (this issue-a, this issue-b). Conversely, no limit on coolant velocity was applied to the inverted geometry since this geometry is assumed to be less affected by vibration phenomena than SC. It should be pointed out, however, that excessive coolant velocity may challenge the structural stability of the twisted tapes in ICTT cores, because of the flow-induced axial forces to which they are subjected. This aspect, not resolved at this stage of the study, needs ultimately to be reviewed.

4.3. CHF constraint during overpower transient

The requirement, for a reactor, to satisfy the DNBR design limit not only during normal operation, but also for all the DNBR-limited transients is often verified by modeling an enveloping transient, which is typically a 112–118% overpower transient (Hejzlar and Todreas, 2000). Consistent with this approach, the present analysis models a transient that, relative to steady state operation, is characterized by an 18% increase in power, 5% reduction in coolant flow rate, and 2 °C increase in coolant inlet temperature. The MDNBR was constrained during this overpower transient. The CHF correlation, used to predict MDNBR, depends on the type of core under investigation, as follows:

- SC: the W3-L correlation was selected because of its frequent use in plant safety analyses (Seabrook, 2002), availability to the public and applicability to square arrays of circular rods supported by grid spacers. While for the W3-L we were not able to find statistics about its accuracy, the original W3 correlation predicts CHF with an average error of −16% and a root-mean-square error of 21.2% (Tong and Tang, 1997).
- IC: the 1995-CHF lookup tables for straight tubes were selected for the IC because they are based on a comprehensive collection of straight tube CHF data spanning our design and operation range. They predict CHF with an average error of 0.69% and a root-mean-square error of 7.82% (Groeneveld et al., 1995).

- ICTT: the CHF vs steam quality lines interpolating Viskanta's experimental data were used (Viskanta, 1961). This interpolation, performed by Viskanta, predicts his experimental CHF values with an average error of −0.58% and a root-mean-square error of 6.32%. The addition of twisted tape inserts is known to enhance CHF performance, but an industry standard CHF correlation for the ICTT design does not exist at the PWR operating pressure. Several CHF correlations exist for circular tubes with twisted tape inserts at lower operating pressures (~1 MPa) (Bergles, 1969; Nariai and Inasaka, 1991; Yin et al., 1994; Tong et al., 1996). Only the data reported by Viskanta (1961), however, were taken at a pressure and mass flux (13.8 MPa and 678–2712 kg/(m² s)) representative of PWR operating conditions (15.5 MPa and 3580 kg/(m² s)). Nevertheless, Viskanta's data refer to an 8 mm channel diameter and do not predict how CHF will vary with diameter: they only show a dependence on the steam quality and on the TT geometric parameter y . Correlations for lower operating pressure suggest a weak dependence of CHF on channel diameter (Bergles, 1969; Nariai and Inasaka, 1991; Yin et al., 1994; Tong et al., 1996). Hence, two approaches are taken for conservatism: (1) assume that CHF is independent of channel diameter and (2) assume that CHF depends on channel diameter as suggested by Groeneveld et al. (1995) for circular tubes without twisted tape:

$$q''_{\text{CHF}}(D_1) = q''_{\text{CHF-8 mm}} \left(\frac{D_1}{8 \text{ mm}} \right)^{-1/3} \quad (2)$$

where $q''_{\text{CHF-8 mm}}$ is the CHF calculated using Viskanta's data, i.e., using approach (1), while D_1 is in mm. The case using the channel diameter dependence is referred to as ICTT $D^{-1/3}$, while that neglecting this dependence simply as ICTT.

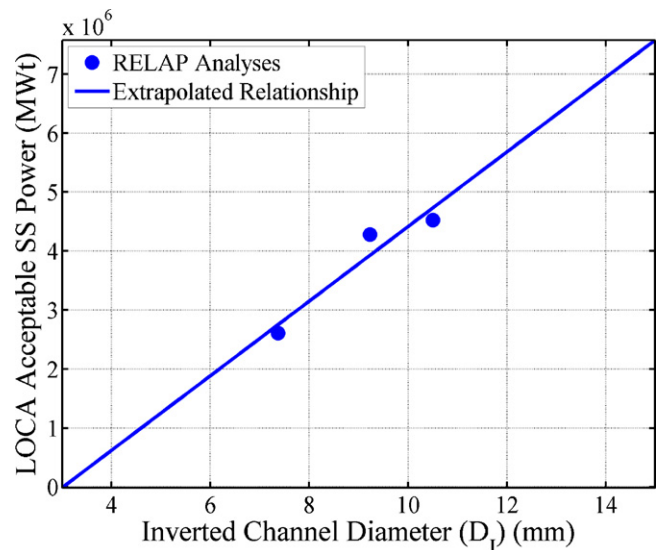


Fig. 3. LOCA acceptable steady state power vs. channel diameter for the inverted geometry.

The MDNBR limit for the SC is assumed to equal the steady state MDNBR of the reference core, which is 1.21 for the W3-L correlation. A similar method for establishing the MDNBR limit for the IC and ICTT designs could not be used because there is not a reference core for the IC and ICTT. A 30% margin in CHF (MDNBR limit = 1.3) was assumed due to variability in Viskanta’s experimental CHF data and accuracy of the Groeneveld look-up tables.

4.4. Cladding temperature constraint during LOCA

An analytical assessment of the LOCA transient using a process developed by Catton et al. (1990) found that U–ZrH_{1.6} fuel in the SC design is not constrained by LOCA performance. These results show that power levels, far higher than those being presented in this comparison, are acceptable (Shuffler et al., this issue-a, this issue-b). This effect is the result of two U–ZrH_{1.6} fuel properties: (1) the higher thermal conductivity of the U–ZrH_{1.6} fuel (~6 times higher than UO₂) yielding lower initial temperatures in the fuel and cladding from stored energy redistribution and (2) lower temperature increases over time from decay heat due to the higher volumetric heat capacity of U–ZrH_{1.6} fuels compared to oxide fuels (~1.2 times higher than UO₂).

Since Catton’s analytical methodology is not directly applicable to the inverted geometry, an IC RELAP (RELAP 3D[®], 2003) model was developed to calculate the maximum clad temperature reached in an IC during LOCA. The RELAP analysis was performed on three inverted geometries of different cooling channel diameter. For these geometries, the power was adjusted until the RELAP calculation yielded a maximum cladding temperature below 1204 °C (USNRC Appendix A LOCA cladding temperature limit) and the fuel quenched to the reflood coolant temperature. The ability to reflood the inverted geometry and quench the fuel was found to be an increasing function of channel diameter, as shown in Fig. 3. The solid line fit to these results was used as an upper limit to the power at a given D₁.

For ICTT the presence of the twisted tape, not modeled in the RELAP analyses described above, may influence the core’s capability to reflood. The twisted tape may in fact hinder the upward steam flow, thus delaying or preventing the reflood of the upper sector of the core. This phenomenon, which will be investigated as future work, could be limited by using partial length twisted tape at the axial location of MDNBR, rather than full length inserts.

Our results, presented next, show that the LOCA constraint is not a governing constraint because the Overpower MDNBR constraint is more limiting. Hence, unless TTs is found to significantly worsen LOCA performance, our results should not be changed by refinement of our methodology with their addition.

5. Results of the parametric studies

Each inverted design geometry has been established by first selecting the fuel area A_F and the fuel to coolant ratio FCR. Then clad thickness t_{clad} and fuel–clad–gap width t_{gap}, the two parameters still needed to fully define the inverted geometry, were calculated using two different approaches. In the first approach, which yielded all the results presented in this paper except for Table 5, the fuel cell geometry was scaled, e.g., the two parameters were determined by linearly scaling based on the fuel cross-sectional area. The results of this approach are referred to in Section 5.1 as the “study with fuel dimensions unconstrained” and are presented in Table 4 in the form of three comparisons:

- comparison A: unconstrained fuel dimension core designs yielding the maximum power;

Table 4
Study 1 – fuel dimensions unconstrained.

Comparison case	Design	Geometric input data				Geometric output data				Core performance output data					
		FCR	A _F (mm ²)	D ^a (mm)	P/D	t _{web} (mm)	t _{clad} (mm)	t _{gap} (mm)	Power ^b (MW _t)	BU ^c (MWD/kg _{HM})	m _{HM} (kg)	T _{cycle} ^d (months)	ΔP (MPa)	T _{Max} ^e (°C)	V (m/s)
(A) Max power	SC	0.47	18.9	5.89	1.42	–	0.41	0.08	5080	128.5	31215	9.6	0.36	517	7.8
	IC	0.30	24.0	10.12	1.14	0.85	0.24	0.08	4246	120.8	25021	8.7	0.09	390	5.7
	ICTT, y = 5.0	0.30	39.2	12.87	1.14	1.08	0.31	0.10	6044	120.8	25021	6.1	0.23	449	8.1
	ICTT, y = 2.5	0.30	45.8	13.92	1.14	1.17	0.33	0.11	6869	120.8	25021	5.4	0.33	482	9.2
(B) Match SC Max power FCR	ICTT, y = 2.5D ^{-1/3}	0.30	39.9	13.04	1.14	1.10	0.31	0.11	6334	120.8	25021	5.8	0.32	456	8.5
	IC	0.47	34.6	9.70	1.22	1.32	0.33	0.05	4055	128.5	31215	12.0	0.11	407	6.3
	ICTT, y = 5.0	0.47	54.8	12.19	1.22	1.66	0.42	0.05	5660	128.5	31215	8.6	0.28	480	8.7
	ICTT, y = 2.5	0.47	65.4	13.26	1.22	1.81	0.46	0.05	6440	128.5	31215	7.6	0.41	527	9.9
(C) Match SC Max power	ICTT, y = 2.5D ^{-1/3}	0.47	57.4	12.49	1.22	1.71	0.43	0.07	5970	128.5	31215	8.2	0.40	496	9.2
	ICTT, y = 5.0	0.76	74.3	11.17	1.35	2.51	0.61	0.06	5080	130.8	40324	12.6	0.38	528	9.6
	ICTT, y = 2.5	1.15	112.1	11.14	1.53	3.76	0.91	0.16	5080	128.6	49538	15.3	0.76	665	12.2
	ICTT, y = 2.5D ^{-1/3}	0.97	94.2	11.12	1.44	3.17	0.76	0.10	5080	129.8	45586	14.2	0.63	595	11.0

^a D for SC is the rod diameter, while D for IC and ICTT is the channel diameter.
^b For the inverted geometry, an inter-assembly gap spacing of 5 mm and an assembly external clad of 4 mm, not modeled in this analysis, will reduce the power by about 10%.
^c BU for 12.5% enriched U–ZrH_{1.6}.
^d Cycle length calculated assuming 3-batch refueling strategy and capacity factor of 0.9.
^e T_{Max} is the maximum fuel temperature in the core (the peak temp of the hot rod at centerline for the SC).

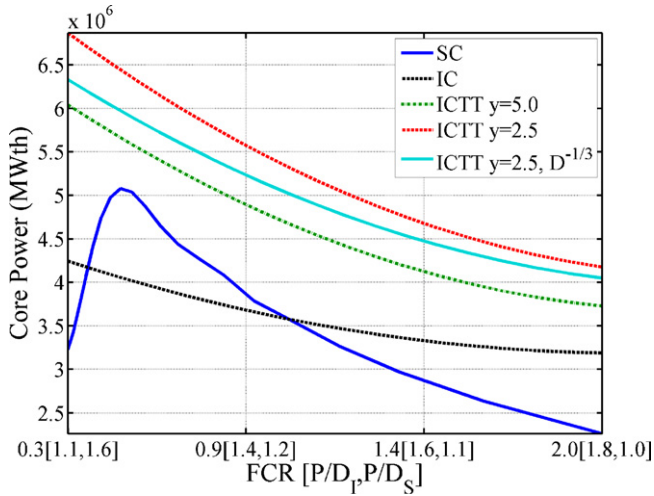


Fig. 4. Core power vs. fuel to coolant ratio.

- comparison B: unconstrained fuel dimension inverted core designs having the same FCR as that of the maximum power SC geometry;
- comparison C: unconstrained fuel dimension inverted core designs having the same power as that of the maximum power SC geometry.

By following the mentioned approach, however, no minimum values of fuel web thickness, clad thickness and fuel–clad–gap width were imposed as constraints. As a consequence, some of the investigated inverted geometries may be difficult to manufacture by conventional means and unable to tolerate the mechanical loads to which they are subjected during operation. To avoid this, and to obtain a preliminary estimate of the inverted geometry performance when manufacturability and mechanical load constraints are considered, t_{clad} , t_{gap} and fuel web thickness were constrained; this constitutes the second approach. This approach was, however, limited to quantitative application of two web thicknesses to a single promising inverted geometry. The results, referred to in Section 5.2 as the “study with fuel dimensions constrained”, are shown in Table 5 and labeled as “comparison D”. The extension of the second approach to the whole inverted geometry spectrum $20 \text{ mm}^2 \leq A_F \leq 150 \text{ mm}^2$ and $0.3 \leq \text{FCR} \leq 2.0$, will be future work for this project.

5.1. Study with fuel dimensions unconstrained

Core power as a function of FCR is shown in Fig. 4. This plot was made by selecting the pitch and diameter that can sustain the highest power for a given FCR. The SC curve peaks at 5080 MW_t for an FCR of 0.5, corresponding to P/D of 1.4. This optimal FCR compares well with that shown in Shuffler et al. (this issue-a, this issue-b), even though the power differs slightly because of the different core height considered (3.66 m in this project, 4.26 m in Shuffler et al., this issue-a, this issue-b). Our simplified vibration constraint and lack of a pressure drop constraint may also lead to deviation between the results. The SC curve has a peak because core power is limited by two separate constraints within the design range, i.e., the overpower MDNBR constraint for FCR < 0.47, and the vibration constraint for FCR > 0.47. The IC and ICTT curves decrease monotonically with increasing FCR because they are only limited by the overpower MDNBR constraint. In agreement with the SC analysis of U–ZrH_{1.6} by Shuffler et al. (this issue-a, this issue-b) and Diller et al. (this issue), the fuel temperature, cladding temperature, and LOCA constraint do not limit the core power for any of the three designs.

Table 5
Study 2—fuel dimensions constrained.

Comparison case	Design	Geometric input data				Geometric output data				Core performance output data					
		FCR	A _F (mm ²)	D (mm)	P/D	t _{web} (mm)	t _{clad} (mm)	t _{gap} (mm)	Power ^a (MW _t)	BU ^b (MWD/kgHM)	m _{HM} (kg)	T _{cycle} ^c (months)	ΔP (MPa)	T _{Max} ^d (°C)	V (m/s)
(D) Constrained fuel dimensions	ICTT y = 2.5	0.54	75.0	13.26	1.30	2	0.76	0.23	5812	129.4	32021	8.7	0.45	616	9.8
	ICTT y = 2.5 D ^{-1/3}	0.54	75.0	13.26	1.30	2	0.76	0.23	5062	129.4	32021	10.0	0.35	582	8.6
	ICTT y = 2.5	0.76	105.7	13.26	1.38	3	0.76	0.23	5250	131.0	40329	12.2	0.46	655	9.9
	ICTT y = 2.5 D ^{-1/3}	0.76	105.7	13.26	1.38	3	0.76	0.23	4500	131.0	40329	14.3	0.35	612	8.5

^a For the inverted geometry, an inter-assembly gap spacing of 5 mm and an assembly external clad of 4 mm, not modeled in this analysis, will reduce the power by about 10%.

^b BU for 12.5% enriched U–ZrH_{1.6}.

^c Cycle length calculated assuming 3-batch refueling strategy and capacity factor of 0.9.

^d T_{Max} is the maximum fuel temperature in the core.

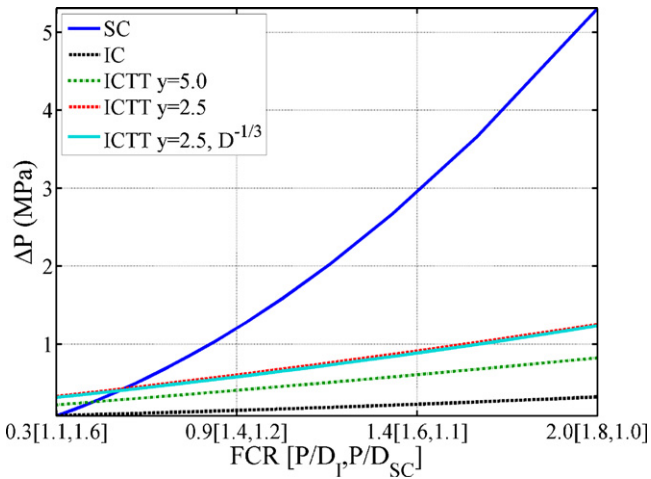


Fig. 5. Pressure drop vs. fuel to coolant ratio.

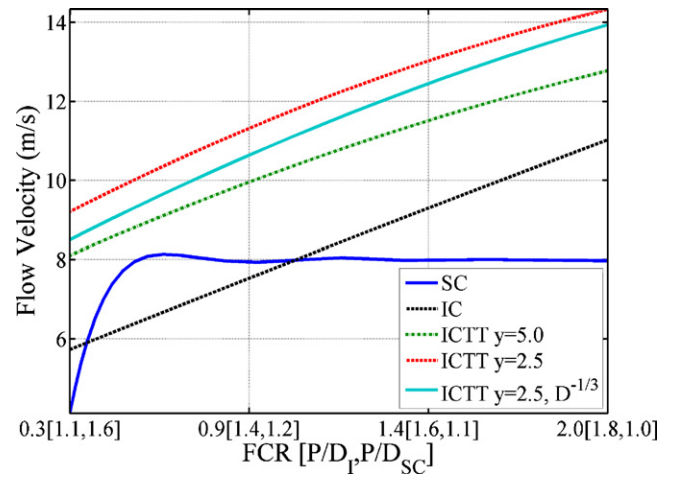


Fig. 6. Average flow velocity vs. fuel to coolant ratio.

The peak powers of the IC, ICTT $y=2.5$, ICTT $y=5.0$, and ICTT $D^{-1/3} y=5.0$ all occur at the smallest FCR considered (FCR = 0.3) and are 4246 MW_t, 6869 MW_t, 6334 MW_t, and 6044 MW_t, respectively. This behavior is consistent with intuition because MDNBR should be more limiting at higher FCRs as the heat is being transferred from more fuel to less coolant, which requires a higher heat flux. The addition of twisted tape offers a substantial power upgrade relative to the SC and IC designs for all FCR. Reducing the value of y from 5.0 to 2.5 enhances CHF, resulting in a ~10% power upgrade for all FCR, albeit at an increased core pressure drop. Whether CHF is independent of channel diameter or proportional to $D^{-1/3}$ from Eq. (2) only results in a 3–7% difference in achievable core power.

Clad thickness and fuel web thickness vary considerably among the designs considered in this study and fuel web thickness in particular falls below an assumed minimum acceptable value (~2 mm, Mattingly et al., 1995) for several geometries. Specific results are presented in Table 4, which identifies three cases of achievable core power structured to assess the economic performance potential of the inverted geometry.

5.1.1. Core pressure drop and coolant velocity

The pressure drop corresponding to the core powers of Fig. 4 is shown in Fig. 5. The pressure drop of all designs increases with increasing FCR, but the SC pressure drop has the strongest dependence. For a given pumping limit, substantially higher FCR are achievable by the inverted designs. The friction component of pressure drop will vary between designs far more than the gravitation and acceleration components, and by the analysis in the Appendix A, we find the ratio of frictional losses between the SC and IC designs to be:

$$\frac{\Delta P_{\text{friction, SC}}}{\Delta P_{\text{friction, IC}}} = \left(\frac{\text{FCR}}{\beta}\right)^{0.6} \quad (3)$$

and the ratio of frictional losses between the SC and ICTT designs to be:

$$\frac{\Delta P_{\text{friction, SC}}}{\Delta P_{\text{friction, ICTT}}} = \left(\frac{1}{1 + (2.752/y^{1.29})}\right) \left(\frac{\pi}{\pi + 2}\right)^{1.2} \left(\frac{\text{FCR}}{\beta}\right)^{0.6} \quad (4)$$

Eqs. (3) and (4) confirm that for increasing FCR the pressure drop of the SC will increase more rapidly than the pressure drop of the IC and ICTT. Grid spacers will generate additional losses in the SC, thereby furthering the advantage of the IC and ICTT designs.

The average coolant velocity corresponding to the core powers of Fig. 4 is shown in Fig. 6. The SC is constrained to flow velocities below 8 m/s and is limited to this value for FCR > 0.6. The coolant

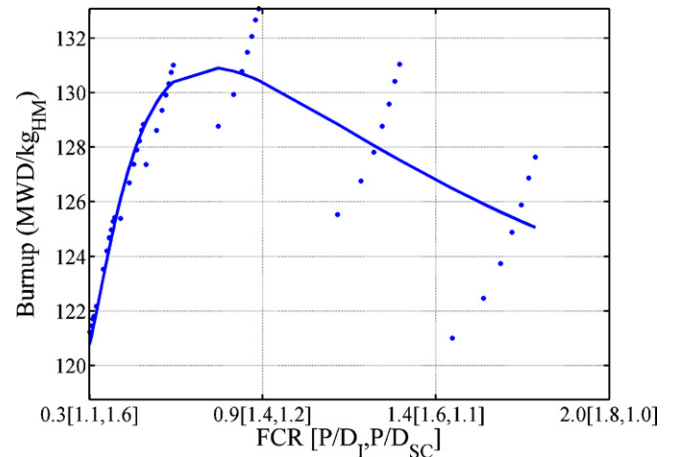


Fig. 7. Neutronically limited discharge burnup vs. FCR for 12.5% enriched U-ZrH_{1.6}.

velocity of the inverted designs increases with FCR due to a reduction in flow area, not offset by the concurrent reduction in core power (and therefore mass flow rate since their ratio is kept constant) as FCR increases. Coolant velocities greater than 12 m/s are needed for high FCR ICTT designs, but the desirable designs presented next are typically in the 10 m/s range.

5.1.2. Discharge burnup and fission gas release

The neutronically limited discharge burnup for standard PWRs from Ganda et al. (this issue) is plotted as a function of FCR in Fig. 7.³ The data points were computed for 12.5% enriched U-ZrH_{1.6} fuel rods in the SC configuration. In this configuration the achievable burnup depends primarily on the fuel to coolant ratio, and secondarily on the rod diameter. The spread within a grouping of data points is caused by varied rod diameter at similar FCR. Inverted fuel is not circular, but since the diameter dependence is small relative to the absolute burnup, a fit line capturing the FCR dependence, but averaging the diameter dependence was used. According to this fit line, the peak burnup is 131 MWD/kg_{HM} at an FCR of 0.8.

The peak fuel temperature of the desirable geometries discussed next is less than 665 °C and their average temperature will be lower than the 650 °C value recommended by Olander et al. (this issue) to

³ In Ganda et al. (this issue) the results in Fig. 7 are plotted as a colormap to explicitly show the dependence on both FCR (P/D) and rod diameter.

Table 6
Summary of the results for economics comparison.

Comparison case	Design	Power ^a (MWt)	Specific power (kW _t /kg _{HM})	T _{cycle} (months)	ΔP (MPa)	V (m/s)	T _{Max} (°C)
(A) Unconstrained geometry—Max power	SC	5080	162.7	9.6	0.36	7.8	517
	IC	4246	169.7	8.7	0.09	5.7	390
	ICTT y = 5.0	6044	241.6	6.1	0.23	8.1	449
	ICTT y = 2.5	6869	274.5	5.4	0.33	9.2	482
	ICTT y = 2.5D ^{-1/3}	6334	253.1	5.8	0.32	8.5	456
(B) Unconstrained geometry—match SC Max power FCR	IC	4055	129.9	12.0	0.11	6.3	407
	ICTT y = 5.0	5660	181.3	8.6	0.28	8.7	480
	ICTT y = 2.5	6440	206.3	7.6	0.41	9.9	527
	ICTT y = 2.5D ^{-1/3}	5970	191.2	8.2	0.40	9.2	496
(C) Unconstrained geometry—match SC Max power	ICTT y = 5.0	5080	126.0	12.6	0.38	9.6	528
	ICTT y = 2.5	5080	102.5	15.3	0.76	12.2	665
	ICTT y = 2.5D ^{-1/3}	5080	111.4	14.2	0.63	11.0	595
(D) Constrained geometry—conservative fuel dimensions	ICTT y = 2.5	5812	181.5	8.7	0.45	9.8	616
	ICTT y = 2.5D ^{-1/3}	5062	158.1	10.0	0.35	8.6	582
	ICTT y = 2.5	5250	130.2	12.2	0.46	9.9	655
	ICTT y = 2.5D ^{-1/3}	4500	111.6	14.3	0.35	8.5	612

^a For the inverted geometry, an inter-assembly gap spacing of 5 mm and an assembly external clad of 4 mm, not modeled in this analysis, will reduce the power by about 10%.

minimize irradiation-induced fuel swelling and fission gas release. Hence, it is possible to attain the burnup shown in Fig. 7.

5.2. Study with fuel dimensions constrained

This study was undertaken since the study discussed in Section 5.1 (fuel dimensions unconstrained) suggests designs with fuel web thickness less than the likely minimum of 2 mm (Mattingly et al., 1995). Specifically, ICTT designs of comparison A are unattainable while designs between those of comparisons B and C ($0.47 < \text{FCR} < 0.76$ –1.15) are likely realizable. Such designs between comparisons B and C will outperform the optimum SC design both in power and in cycle length. In particular, it can be noticed that the ICTT geometry having $y = 2.5$ and $D = 13.26$ mm is simultaneously characterized by a high attainable power and a reasonably large web thickness (comparison B, design ICTT $y = 2.5$). This geometry was chosen as a starting point on which the constraints on fuel, gap and clad were applied, i.e., comparison D constrained fuel dimensions. For comparison D web thicknesses of 2 mm and 3 mm were considered, each having gap and clad thicknesses of 0.23 mm and 0.76 mm, respectively. These dimensions for clad and gap were obtained by using scaling correlations suggested by Garkisch and Petrovic (2004) for hydride fuels; however, due to the uncertainty in hydride fuel swelling, the gap thickness derived from these correlations was conservatively doubled.

The results for these cases are presented in Table 5. The spread between the lowest to the highest power cases, 4500–5812 MW_t, brackets accommodation of reasonably expected fuel behavior and CHF performance. To secure a power advantage compared to the optimum SC (5080 MW_t) it is sufficient that either the CHF does not significantly depend on cooling channel diameter or that the fuel perform better than the most conservative result (4500 MW_t), i.e., case of 5250 MW_t (no diameter dependence of CHF) or 5812 MW_t (fuel web performance improved).

6. Economic benefits of the inverted design

An economic analysis of the inverted design has not been completed, but the thermal hydraulic results presented here and the neutronic results from Ganda et al. (this issue) were used to assess its economic viability relative to the standard design. Shuffler et al. (this issue-a, this issue-b) reports that the optimal enrichment for U–ZrH_{1.6} is 12.5%, and this enrichment has therefore been used for our comparison of the standard and inverted designs.

6.1. Factors influencing cost of electricity

The cost of electricity is dominated by three major factors: power density (affecting capital cost), specific power (affecting fuel cycle cost) and cycle length (affecting operations and maintenance cost). The ideal design would concurrently maximize these three factors to reduce the cost of electricity. Nevertheless, the contrasting requirements of thermal hydraulic, neutronic, and fuel performance constraints demand compromise such that each critical factor is not optimized. The sought economic compromise was determined for U–ZrH_{1.6} and UO₂ cores supported by grids and wire wraps (Shuffler et al., this issue-a, this issue-b) in previous studies. Our exploration here of the inverted design has not determined its optimum configuration but instead suggests a range of inverted designs that will concurrently outperform the SC in core power, specific power, and cycle length.

The economic comparison discussed here does not account for research and development (R&D) costs of the inverted design, which are expected to be large, since it is assumed that, like the standard design, the inverted design is also widely deployed. In this scenario, since R&D costs are spread over all the future cores, they do not substantially affect the cost of electricity.

6.2. Cost comparison

Factors influencing the cost of electricity are presented in Table 6 for comparisons A–D. Power density for all cases is reflected by core power since core volume is held constant.

- For comparison A, the ICTT geometries clearly offer higher power density and specific power than the SC, but a concurrent reduction in cycle length. Core pressure drops of the highest power cases are similar to the SC which is 0.36 MPa, but 65% higher than the reference oxide SC (~0.2 MPa). Maximum fuel temperatures are well below the 750 °C limit.
- For comparison B, the FCR, BU, and m_{HM} of the inverted geometries are the same as the maximum powered SC, but power increases are only attainable by the ICTT geometries. Cycle lengths are small for ICTT geometries. Each of the ICTT geometries of comparison B offers a significant power upgrade relative to the SC, with acceptable maximum fuel temperature and pressure drops ranging between –27% and +14% with respect to the SC.
- For comparison C, the power of the inverted geometries is taken the same as the maximum powered SC, but the ICTT geometries

offer increased FCR, BU, and m_{HM} . Resulting specific power values are lower than for the SC while cycle lengths are higher. Fuel temperatures are again acceptable. The pressure drop requirements of the ICTT $y = 2.5$ and ICTT $y = 2.5 D^{-1/3}$ designs may be prohibitive if development of pumping technology capable of increased head and flow rate requires significant capital investment.

- For comparison D, again the 2 mm fuel web thickness configurations exhibit specific power and power density which range from high to about equal relative to the SC. Cycle lengths and pressure drops are comparable to the SC. Fuel temperatures are high but acceptable.

7. Recommended future work

The following future work, in order of highest priority, is required to confirm the inverted core thermal hydraulic and fuel performance claimed by this study. However, the feasibility of the inverted core also depends on neutronics and economics, not yet investigated. These aspects will need to be studied if the results obtained through the analyses listed below will prove that the thermal hydraulic and fuel performance claimed in this paper are achievable.

- Extension of the methodology constraining t_{web} , t_{clad} and t_{gap} to the whole inverted geometry spectrum.
- Assessment of the inverted fuel assembly manufacturability.
- Measurement of CHF in circular tubes with twisted tape inserts at high pressure ($P \sim 15.5$ MPa) and high flow rate ($Re \sim 800,000$). Our literature search only found Viskanta's (1961) data to be within this pressure range. Due to a lack of data at high Re , we were forced to extrapolate Viskanta's CHF data to high Re , and we would like to confirm this extrapolation by experiment. Additionally, we would like to study partial length twisted tape inserts, which are positioned only in the axial regions of high CHF. Partial length inserts would offer the CHF benefits, with reduced pressure drop.
- Analysis of twisted tape inserts detachment and erosion. Twisted tape inserts need to be robustly designed to resist detachment and erosion due to high flow velocity. A quantitative assessment of vibration and erosion will be necessary to adequately design and attach the twisted tape inserts.
- Development of control rod design.
- Fuel temperature distribution evaluation of the actual inverted geometry to replace the equivalent annulus approximation used here.
- A more detailed transient and accident analyses. The post-LOCA reflooding analysis herein needs to be extended to a larger tube diameter range, at several FCRs. In addition, transient flow instabilities that may arise from the blockage of one or more non-communicating channels during steady state operation need to be studied. Beyond design basis accidents ultimately need to be considered.
- A more detailed collection of fission gas release and irradiation-induced swelling data for U–ZrH_{1.6} fuel at high burnup and high temperature.

8. Conclusions

The thermal hydraulic performance of U–ZrH_{1.6}-fueled inverted core designs with and without twisted tape were estimated and compared to those of the standard rod bundled core design also fueled with U–ZrH_{1.6}. Neutronic feasibility of the inverted design was not established. It was found that inverted cores without twisted tape do not offer power upgrades relative to the standard design. The use of twisted tape increases the CHF of the inverted design and thereby permits higher steady state core pow-

ers than can be realized by the standard design. Higher power, burnup, and heavy metal loading can be concurrently achieved by the inverted core with twisted tape relative to the optimal standard core. The power of the current optimal inverted design with twisted tape, which has, however, fuel web and clad thickness just below our acceptable ranges, is 6869 MW_t, which is 135% of the optimally powered U–ZrH_{1.6} standard design (5080 MW_t—determined herein). This may imply potential economic advantages for inverted core designs. Upon design optimization using reasonable values for fuel web and clad thickness we expect the inverted design power to be slightly reduced.

Appendix A. Derivation of geometric relationships

A.1. Cladding and gap thickness

For all the standard and inverted geometries considered for Study 1, constant ratios between the fuel area A_F and (1) the combined fuel + gap area A_{FG} and (2) the combined fuel + gap + clad area A_{FGC} were assumed throughout the analysis. The numerical values of these ratios were obtained by extending geometric relations valid for a typical pin geometry PWR core to any SC geometry and inverted geometry considered in Study 1, as explained as follows. If, for a SC geometry, fuel–clad–gap and clad thicknesses are assumed to be proportional to the pellet diameter according to typical dimensions in oxide fueled PWRs, i.e.:

- a) gap thickness = 1.3% of the pellet diameter;
- b) clad thickness = 7% of the pellet diameter.

then the fuel rod outer diameter is a constant multiple of the pellet diameter:

$$D_{SC} = 2D_{F,SC}(0.013 + 0.07) + D_{F,SC} = 1.166D_{F,SC} \quad (5)$$

and the combined cross-sectional area of the fuel and gap (A_{FG}) is a constant multiple of the area of the fuel alone:

$$\begin{aligned} A_{FG} &= \frac{\pi(D_{F,SC} + 2t_{gap})^2}{4} = \frac{\pi(D_{F,SC} + 2 \times 0.013D_{F,SC})^2}{4} \\ &= 1.053 \frac{\pi D_{F,SC}^2}{4} = 1.053A_F \end{aligned} \quad (6)$$

The reciprocal of the lead coefficient 1.053 in Eq. (6) is referred to as α and represents the area ratio A_F/A_{FG} . It is equal to 0.950. Similarly, using Eq. (5), the combined cross-sectional area of fuel + gap + clad can be related to the fuel area only by means of the following:

$$A_{FGC} = \frac{\pi D_{SC}^2}{4} = \frac{\pi(1.166D_{F,SC})^2}{4} = 1.36A_F \quad (7)$$

where the reciprocal of the lead coefficient is referred to as β , and is equal to 0.736. These values of α and β are maintained constant for all the standard and inverted designs considered in Study 1, therein dictating the gap and cladding thicknesses.

A.2. Core pressure drop

Here we compare the characteristic frictional pressure drop for inverted and standard designs. Frictional pressure drop is related to equivalent diameter as follows:

$$\Delta P_{friction} = f \left(\frac{L}{D_e} \right) \frac{\rho V^2}{2} \quad (8)$$

where L is the core length, V is the flow velocity, and the friction factor, f , can be estimated using McAdams empirical result for straight tubes:

$$f_s = 0.184Re^{-.2} \quad (9)$$

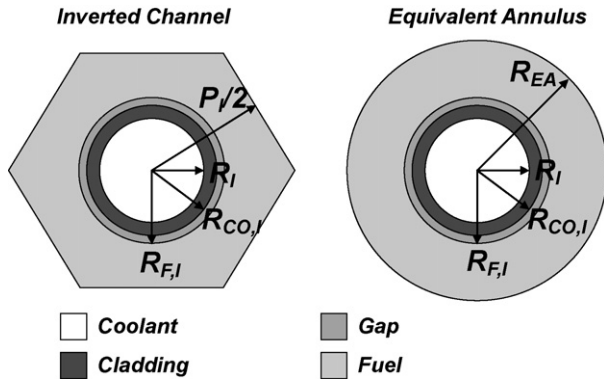


Fig. 8. Transformation between inverted channel and equivalent annulus for calculation of fuel temperature distribution in the inverted design.

Although the effect of surface roughness is neglected for the following scaling argument, it was considered in our analysis by use of the Colebrook equation (Colebrook, 1939). From Eqs. (8) and (9), the straight tube frictional pressure drop scales with hydraulic diameter as follows:

$$\Delta P_{\text{friction}} = 0.184 \left(\frac{\rho V D_e}{\mu} \right)^{-0.2} \left(\frac{L}{D_e} \right) \frac{\rho V^2}{2} \quad (10)$$

For the average channel, the ratio of frictional pressure drops exhibited by SC and IC designs with equivalent FCR, A_f , L and flow velocity (and therefore core power since the core enthalpy rise is maintained constant in this analysis) is given by:

$$\frac{\Delta P_{\text{friction,SC}}}{\Delta P_{\text{friction,IC}}} = \left(\frac{D_{e,IC}}{D_{e,SC}} \right)^{1.2} \quad (11)$$

which becomes, using the relation shown in Table 1:

$$\frac{\Delta P_{\text{friction,SC}}}{\Delta P_{\text{friction,IC}}} = \left(\frac{\text{FCR}}{\beta} \right)^{0.6} \quad (12)$$

The ratio of frictional pressure drops exhibited by SC and ICTT designs with equivalent FCR, A_f , L and flow velocity (and therefore core power) can be obtained using the relations shown in Table 1 together with Eq. (10):

$$\begin{aligned} \frac{\Delta P_{\text{friction,SC}}}{\Delta P_{\text{friction,ICTT}}} &= \left(\frac{1}{1 + (2.752/y^{1.29})} \right) \left(\frac{D_{e,ICTT}}{D_{e,SC}} \right)^{1.2} \\ &= \left(\frac{1}{1 + (2.752/y^{1.29})} \right) \left(\frac{\pi}{\pi + 2} \right)^{1.2} \left(\frac{\text{FCR}}{\beta} \right)^{0.6} \end{aligned} \quad (13)$$

A.3. Equivalent annulus approximation for inverted design

The equivalent annulus approximation was used to determine the temperature distribution within the inverted fuel. Fig. 8 shows the inverted channel and equivalent annulus. R_i , R_{ci} , and R_{co} are the same for both. The value of R_{EA} is chosen so that the fuel cross-sectional area in the equivalent annulus is the same as that in the actual inverted cell. By means of simple geometric relations it can

be shown that:

$$R_{EA} = P_1 \sqrt{\frac{\sqrt{3}}{2\pi}} = \sqrt{\frac{A_{f,I}}{\pi} \left(\frac{1}{\beta} + \frac{1}{\text{FCR}} \right)} \quad (14)$$

References

Bergles, A.E., 1969. Survey and evaluation of techniques to augment convective heat and mass transfer. *Progress in Heat and Mass Transfer* 1, 331–424.

Catton, I., et al., 1990. Quantifying reactor safety margins. Part 6. Physically based method of estimating PWR large break loss of coolant accident PCT. *Nuclear Engineering and Design* 119, 109–117.

Colebrook, C.F., 1939. Turbulent flow in pipes with particular reference to the transition region between the smooth and rough pipe laws. *Proceedings of the Institution of the Civil Engineers* 11, 133.

Diller, P., et al., this issue. Thermal hydraulic analysis for hydride-fueled wire wrapped PWR cores. *Nuclear Engineering and Design*.

Ganda, F., et al., this issue. Reactor physics analysis for hydride-fueled PWR cores. *Nuclear Engineering and Design*.

Garkisch, H.D., Petrovic, B., 2004. Proposed correlation for cladding thickness and fuel-cladding gap for UO_2 and U-ZrH fuel in PWRs. Westinghouse Electric Company, NERI02-189-WEC-04, Rev. 2, December 13, 2004.

Greenspan, et al., this issue. Hydride fuel for LWRs—project overview. *Nuclear Engineering and Design*.

Groeneveld, et al., 1996. The 1995 look-up table for critical heat flux in tubes. *Nuclear Engineering and Design* 163, 1–23.

Hejzlar, P., Todreas, N.E., 2000. Response to Letter to the Editor on the round table discussion on reactor power margins published in *Nuclear Engineering and Design* 163 (1–2) 1996. *Nuclear Engineering and Design* 201, 347–352.

Lillie, A.F., McClelland, D.T., Roberts, W.J., Walter, J.H., 1973. Zirconium hydride fuel element performance characteristics. AIAEC13084. Atomic International Division, Canoga Park, CA, USA.

Malen, J.A., et al., 2004. Thermal hydraulic design of hydride fueled PWR cores. In: *Proceedings of the 6th International Conference on Nuclear Thermal Hydraulics, Operations and Safety*, Nara, Japan, October 4–8.

Manglik, R.M., Bergles, A.E., 1993. Heat transfer and pressure drop correlations for twisted-tape inserts in isothermal tubes. Part II. Transition and turbulent flows. *Journal of Heat Transfer* 115, 890–896.

Mattingly, B.T., Hejzlar, P., Todreas, N.E., Driscoll, M., 1995. Fuel matrices for the passive pressure tube light water reactor, Massachusetts Institute of Technology, Program for Advanced Nuclear Power Studies, Report No. MIT-ANP-TR-031, June.

Nariai, H., Inasaka, F., 1991. Critical heat flux of subcooled flow boiling in tubes with internal twisted tapes. In: *Proceedings of the 7th Nuclear Thermal Hydraulics*, San Francisco.

NRC 10CFR50.46. US Nuclear Regulatory Commission Regulations, Title 10 Code of Federal Regulations, Part 50-Domestic Licensing of Production and Utilization Facilities. August 28, 2007.

Olander, D., et al., this issue. Uranium–zirconium hydride fuel properties. *Nuclear Engineering and Design*.

Pope, M.A., Yarsky P.J., Driscoll M.J., Hejzlar P., Saha P., 2005. An Advanced Vented Fuel Assembly Design for GFR Application, vol. 92. *ANS Transactions*, San Diego, USA, p. 211, June 5–9, 2005.

RELAP, 2003. RELAP 3D Code Manual. Volume 5: User’s Guidelines. Idaho National Laboratory. Revision 2.3. Idaho Falls, ID.

Seabrook Power Station Updated Final Safety Analysis Report (UFSAR), 2002. Revision 8, 2002.

Shuffler, C., et al., this issue. Thermal hydraulic analysis for grid supported pressurized water reactor cores. *Nuclear Engineering and Design*.

Shuffler, C., et al., this issue. Economic analysis of grid and wire wrap supported hydride and oxide fueled PWRs. *Nuclear Engineering and Design*.

Simnad, M.T., 1981. The U-ZrH_x alloy: its properties and use in TRIGA fuel. *Nuclear Engineering and Design* 64 (1981), 403–422.

Stewart, C., 1985. VIPRE-01: A Thermal Hydraulic Code for Reactor Cores. Vol. 3, Programmer’s Manual.

Tong, L.S., Tang, Y.S., 1997. *Boiling Heat Transfer and Two-Phase Flow*, 2nd ed. Taylor and Francis.

Tong, W., Bergles, A.E., Jensen, M.K., 1996. Critical heat flux and pressure drop of subcooled flow boiling in small-diameter tubes with twisted-tape inserts. *Journal of Enhanced Heat Transfer* 3 (2), 95–108.

Viskanta, R., 1961. Critical heat flux for water in swirling flow. *Nuclear Science and Engineering* 10, 202–203.

Yin, S.T., et al., 1994. Assessment of a heat transfer correlations package for water-cooled plasma-facing components in fusion reactors. *Nuclear Engineering and Design* 146, 311–323.